ORIGINAL SCIENTIFIC PAPER

CROATICA CHEMICA ACTA

Croat. Chem. Acta **2026**, *99*(3)
Published online: November 19, 2026
DOI: 10.5562/cca4316

HKD 1926

Hydrogen Bonding and Noncovalent Interactions in Scopoletin–Water Complexes: A DFT and Topological Study

Harjinder Singh

Multani Mal Modi College, Department of Chemistry, Near Sunami Gate, Lower Mall Patiala, 147001, Punjab, India
Corresponding author's e-mail address: drharjinder04@gmail.com

RECEIVED: March 03, 2026 ✯ REVISED: September 08, 2026 ✯ ACCEPTED: September 09, 2026

Abstract: The interaction between scopoletin and water was investigated using density functional theory (DFT) calculations. The results show that the scopoletin–water complexes are stabilized predominantly by non-covalent interactions, particularly hydrogen bonding. Among the five investigated conformations, **C2** exhibits the most negative BSSE- and ZPE-corrected interaction energy, indicating the strongest intermolecular interaction among the conformers examined. The complexes were analyzed using natural population analysis (NPA), natural bond orbital (NBO) analysis, reduced density gradient (RDG) analysis, and quantum theory of atoms in molecules (QTAIM) to gain deeper insight into the nature of the intermolecular interactions. The results indicate that the hydrogen-bonding interactions in **C2** are stronger and more directional than those in the other investigated conformers, whereas **C1** exhibits comparatively weaker intermolecular interactions. The positive Laplacian values at the bond critical points are consistent with the closed-shell and predominantly electrostatic character of these hydrogen bonds, with limited covalent contribution. Overall, this study provides detailed molecular-level insight into the microsolvation of scopoletin and highlights the important role of hydrogen bonding in determining the relative interaction strengths of scopoletin–water conformers.

Keywords: scopoletin, hydrogen bonding, water–solute interactions, density functional theory, non-covalent interactions.

INTRODUCTION

SCOPOLETIN or 7-hydroxy-6-methoxy-2H-chromen-2-one is a naturally occurring coumarin derivative[1] widely found in medicinal plants and is known for a range of biological activities, including antioxidant, anti-inflammatory, antimicrobial, hepatoprotective, and anticancer effects.[2] These biological properties are closely related to the molecular structure of scopoletin and its ability to participate in noncovalent interactions with its surrounding environment, particularly solvent molecules.[3] Water plays a crucial role in determining the stability, solubility, conformational behaviour, and reactivity of bioactive compounds.[4] Interactions between solutes and water molecules influence hydrogen-bonding patterns, redistribute electronic charge, and affect molecular recognition processes in biological systems. In the case of phenolic and coumarin-based molecules, hydrogen bonding with water and other solvents can lead to noticeable changes in charge distribution and molecular geometry, which in turn can modify physicochemical properties and biological activity.[5] Despite the importance of these interactions, detailed molecular-level studies focusing on the interaction between scopoletin and water are still limited.

Density functional theory (DFT) has proven to be a reliable computational approach for investigating weak intermolecular interactions in molecular complexes.[6-7] DFT methods allow accurate optimization of molecular geometries and evaluation of interaction energies, making them particularly suitable for hydrogen-bonded systems. However, interaction energies alone are often insufficient to fully describe the nature of noncovalent interactions. For this reason, complementary analytical techniques are commonly employed. Natural population analysis (NPA) provides insight into charge redistribution and polarization effects upon complex formation, while natural bond orbital (NBO) analysis offers a quantitative description of

This work is licensed under a Creative Commons Attribution 4.0 International License.

donor–acceptor interactions and charge-transfer processes such as n→σ* and n→π* delocalization.[8-9] In addition, reduced density gradient (RDG) and noncovalent interaction (NCI) analyses enable visualization of weak interactions in real space, allowing attractive, dispersive, and repulsive regions to be clearly distinguished.[10-11] In addition, the quantum theory of atoms in molecules (QTAIM) provides a rigorous topological framework for characterizing hydrogen bonds through bond critical points and associated electron density descriptors.[12-13] Previous computational studies have demonstrated that a combined analysis using NBO, RDG/NCI, and QTAIM methods yields a comprehensive and reliable description of hydrogen bonding and weak intermolecular interactions with water.[14-16] However, such an integrated theoretical approach has not yet been systematically applied to the scopoletin–water system.

In this work, a detailed DFT-based investigation of the interaction between scopoletin and a single water molecule was carried out. Five low-energy conformations of the scopoletin–water complex were identified and optimized. Their relative interaction strengths were assessed using BSSE- and ZPE-corrected interaction energies, and the nature of intermolecular interactions is examined using electrostatic potential analysis, NPA, NBO, RDG/NCI, and QTAIM methods. By correlating energetic, electronic, and topological descriptors, this study aims to give clear molecular-level understanding of water–scopoletin interactions and to elucidate the role of hydrogen bonding in governing conformational preference and stabilization.

COMPUTATIONAL METHODS

The DFT calculations were carried out using the Gaussian 09 program package without imposing any geometrical constraints. Geometry optimizations were performed employing the B3LYP-D3(BJ) hybrid dispersion-corrected functional in conjunction with the 6-311++G(d,p) basis set.[17] The interaction energies were corrected for basis set superposition error (BSSE) using the counterpoise method (Counterpoise = 2). Zero-point vibrational energy (ZPE) corrections were obtained from frequency calculations and incorporated into the interaction energies to obtain more reliable energetic parameters.[17] Molecular structures were visualized using GaussView 06.[18] Molecular electrostatic potential (ESP), Natural population analysis (NPA), Reduced Density Gradient (RDG), and Quantum Theory of Atoms in Molecules (QTAIM) analyses were carried out using the Multiwfn program,[19] while graphical visualization of RDG isosurfaces and topological features were performed with VMD software.[20] Within the RDG approach, the electron density function $\rho(r)$ was obtained directly from the DFT wavefunction.[21] The reduced density gradient, RDG(r), was calculated using the electron density and its first derivative according to the following equation:

$$\mathrm{RDG}(r) = \frac{|\nabla\rho(r)|}{2(3\pi^2)^{1/3}\,\rho(r)^{4/3}} \quad (1)$$

Scatter plots of the reduced density gradient (RDG) as a function of the electron density weighted by the sign of the second eigenvalue of the Hessian matrix, sign(λ_2)ρ, were used to analyze the nature of intermolecular interactions in the system. In these plots, regions with positive sign(λ_2)ρ values correspond to repulsive interactions and appear as red spikes, whereas attractive interactions, particularly hydrogen bonding, are characterized by negative sign(λ_2)ρ values and are represented by blue spikes. Weak dispersive interactions, such as van der Waals forces, are observed near sign(λ_2)$\rho \approx 0$ and appear as green features. The position and intensity of these spikes provide qualitative information on the strength and type of noncovalent interactions present in the complex.[21] QTAIM analysis was used to further classify bonding interactions based on topological parameters evaluated at bond critical points (BCPs). Covalent interactions are characterized by relatively high electron density (ρ) and negative Laplacian values ($\nabla^2\rho$) at the BCP, whereas noncovalent interactions exhibit low electron density and positive $\nabla^2\rho$ values. In addition, the local electronic energy density at the BCP (H_{BCP}), together with $\nabla^2\rho$, was used to distinguish between covalent ($\nabla^2\rho_{BCP} < 0$ and $H_{BCP} < 0$), partially covalent or electrostatic (($\nabla^2\rho_{BCP} > 0$ and $H_{BCP} < 0$), and purely electrostatic interactions ($\nabla^2\rho_{BCP} > 0$ and $H_{BCP} > 0$).[22]

RESULTS AND DISCUSSION

We have investigated intermolecular interaction between scopoletin and water using Density Functional Theory (DFT) calculations. Firstly, in order to identify favorable interaction sites between scopoletin and water, their individual structures were optimized using DFT at B3LYP-D3 (BJ)/6-311++G (d, p) level of theory in gas phase. The ZPE corrected electronic energy of optimized structures (Figure 1) of scopoletin and water were found to be –686.639392 Hartree and –76.437748 Hartree, respectively.

The Natural Population Analysis (NPA) is an important method to find reactive sites and molecular interactions based upon the natural bond orbitals rather than the Mulliken population which is affected by basis set used.[23] The NPA analysis of isolated water molecule shows that it exhibits a highly electronegative oxygen atom (–0.997 e) and two electropositive hydrogens (+0.499 e each), indicating its ability to function both as a hydrogen-bond donor and acceptor. In scopoletin, oxygen atoms O10,

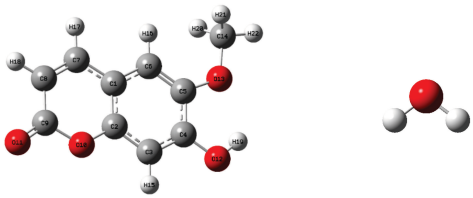


Figure 1. Optimized structures of scopoletin and water molecules at B3LYP-D3 (BJ)/6-311++G (d, p) level of theory in gas phase.

O11, O12, O13 carry significant negative charges ranging from –0.50e to –0.70e, while carbonyl carbon C9 (+0.75 e) and hydroxyl hydrogen H19 (+0.52e) appear as strong electrophilic centers. The results are consistent with typical NPA charges reported for an isolated water molecule and systems similar to scopoletin at the DFT level.[23] These charge distributions suggest that hydrogen atoms of water are likely to form hydrogen bonds with the electronegative oxygens of scopoletin (notably O10 and O13), while the lone pairs of water oxygen may interact weakly with the electron-deficient region near C9 and H19.

Further, in order to identify the electron-rich and electron-deficient regions, to find possible orientation between two molecules, electrostatic potential (ESP) analyses[24] were performed on isolated scopoletin and on water molecule. The electrostatic potential surface of both individual molecules mapped over the Van der Waals surface was calculated with DFT calculations using their optimized structure and are shown in Figure 2.

For the water molecule, the ESP surface displays a pronounced negative potential (−37.42 kcal/ mol) localized around the oxygen atoms (O23) as blue region, while both hydrogen atoms (H24, H25) exhibit positive potentials (+46.47 kcal/mol) in the red zones. This polarity reflects water's dual role as a hydrogen-bond donor (via its H atoms) and acceptor (via its O atom). In the scopoletin molecule, regions of strong negative electrostatic potential are observed near the oxygen atom of the carbonyl group (O11) and hydroxyl oxygen atom (O12) (−45.16 kcal/mol and −21.71 kcal/mol), indicating these are the most likely hydrogen-bond acceptor sites. Conversely, positive potential regions around the hydroxyl hydrogen H19 (+47.15 kcal/mol) and near the methoxy group (+28.13 kcal/mol) correspond to hydrogen-bond donor sites or electrophilic centers capable of interacting with electron-rich areas of water.

Based upon interaction sites predicted by NPA and ESP analysis a systematic conformational analysis of the scopoletin–water complex was performed. The water molecule was initially placed near all potential hydrogen-bond donor and acceptor sites of scopoletin with different orientations. Five plausible initial structures (**C1–C5**) were subsequently optimized without imposing any geometrical constraints at the B3LYP-D3(BJ)/6-311++G(d,p) level of theory in gas phase. The optimized conformations are shown in Figure 3. The interaction (binding) energy between scopoletin and water was calculated using the equation, $\Delta E_{\text{int}}^{\text{CP}} = E_{\text{conformation}} - (E_{\text{scopoletin}} + E_{\text{water}}) + E_{\text{BSSE}}$, where $E_{\text{conformation}}$ is the ZPE-corrected total electronic energy of the optimized scopoletin–water complex (**C1–C5**), $E_{\text{scopoletin}}$ and E_{water} are the ZPE-corrected total electronic energies of the optimized isolated scopoletin and water molecules, respectively, and E_{BSSE} is the Basis Set Superposition Error correction term calculated via the counterpoise method. The ZPE-corrected total electronic energies corresponding to the optimized geometries of the scopoletin–water complexes, together with the BSSE- and ZPE-corrected interaction energies, are summarized in Table 1.

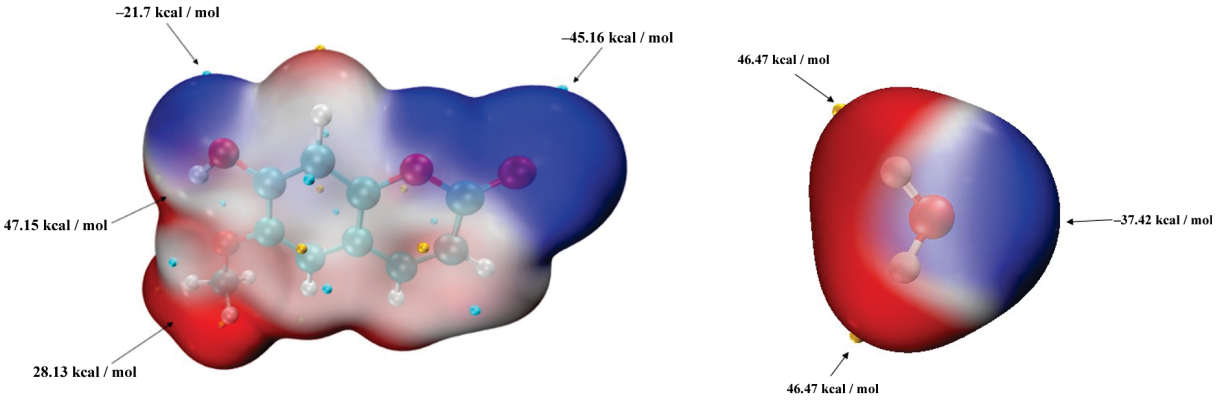


Figure 2. ESP analysis of scopoletin and water molecule drawn over the Van der Waals surface with BWR (blue, white, red) colour scheme (blue – negative potential region, white – zero electrostatic potential, and red – positive electrostatic potential).

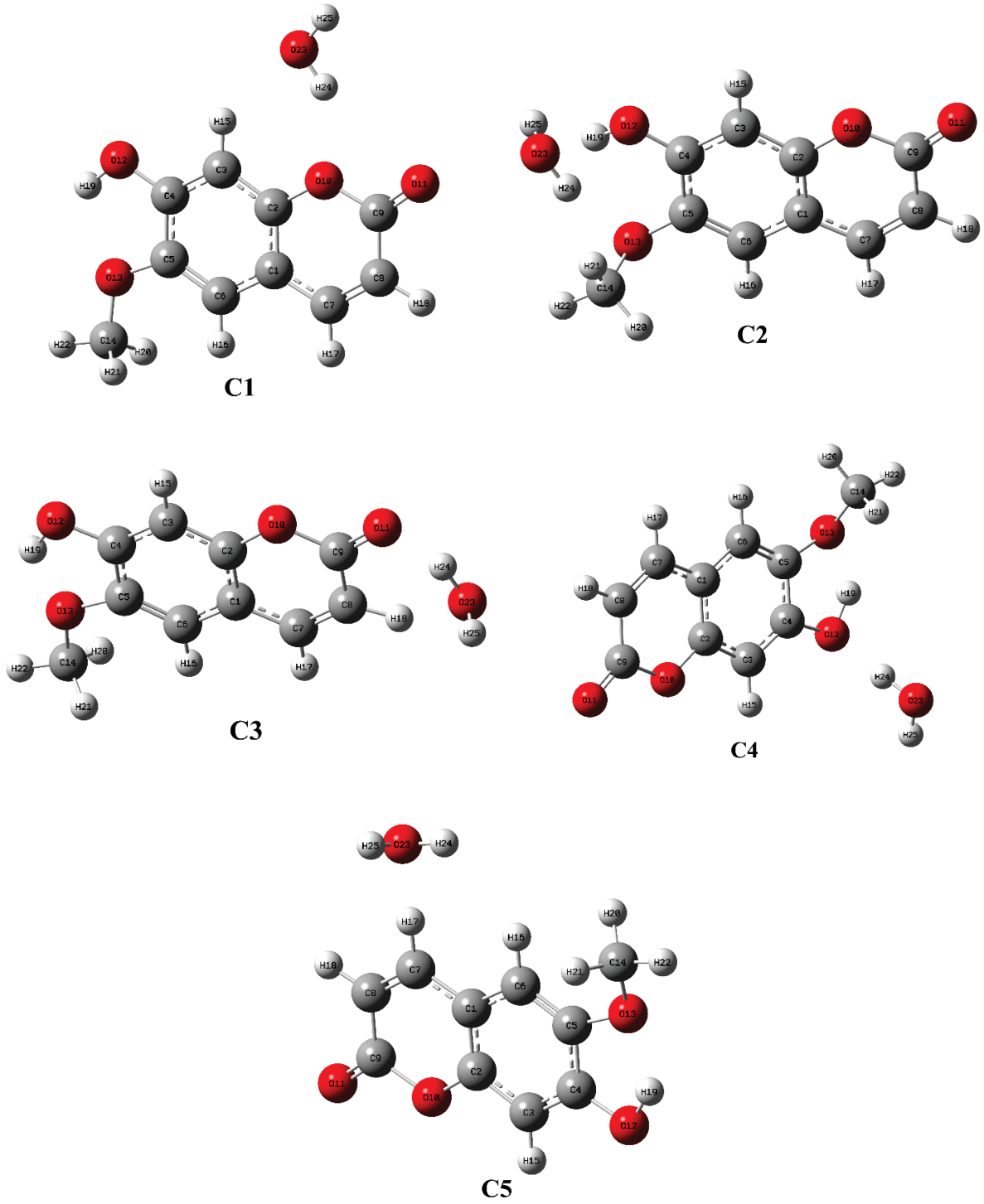


Figure 3. Optimized structures of scopoletin-water complexes **C1**–**C5** at B3LYP-D3 (BJ)/6-311++G (d, p) level of theory in gas phase.

Frequency calculations confirmed that all five optimized structures correspond to local minima on the potential energy surface, as indicated by the absence of imaginary frequencies, shows that several binding motifs are possible for the scopoletin–water complex. However, significant differences in interaction energies were observed. Among

Table 1. Total ZPE corrected electronic energies of the optimized scopoletin–water complexes (**C1–C5**) and the corresponding BSSE- and ZPE-corrected interaction energies.

conformation	ZPE Corrected Electronic Energy (Hartree)	BSSE Corrected Interaction Energy (kcal/mol)
C1	–763.085889	–4.78
C2	–763.088184	–6.08
C3	–763.083865	–3.65
C4	–763.084152	–4.02
C5	–763.079339	–1.07

the investigated conformers, **C2** exhibits the most negative interaction energy (−6.08 kcal/mol), indicating the strongest intermolecular interaction among the conformers examined. Conformer **C1** is the second most stable with an interaction energy of −4.78 kcal/mol, followed by **C4** (−4.02 kcal/mol) and **C3** (−3.65 kcal/mol). In contrast, **C5** possesses the weakest interaction energy (−1.07 kcal/mol), suggesting considerably weaker stabilization due to less favorable hydrogen-bonding interactions. The enhanced stability of **C2** can be attributed to more effective hydrogen-bonding interactions between the hydroxyl hydrogen (H19) and oxygen atom of methoxy group (O13) of scopoletin and the oxygen (O23) and hydrogen (H24) of the water molecule. In contrast, **C1** represents a slightly less favorable arrangement with weaker hydrogen bonding and suboptimal dipole alignment. Although several local minima were identified, the interaction energy analysis indicates that **C1** and **C2** are the two most strongly bound conformers among the binding motifs examined.

In order to investigate the effect of the solvent environment on the stability of the scopoletin–water complexes, calculations were performed using the Polarizable Continuum Model (PCM) with water as the implicit solvent[25] at the B3LYP-D3(BJ)/6-311++G(d,p) level of theory. The calculated BSSE and ZPE-corrected interaction energies for conformers **C1** and **C2** were found to be –5.03 kcal/mol and –6.95 kcal/mol, respectively. Although the solvent environment slightly modifies the interaction energies relative to the gas-phase calculations, **C2** exhibits a more negative interaction energy than **C1** in the PCM aqueous environment. These results indicate that the stronger hydrogen-bonding network in **C2** is preserved in the aqueous environment. Nevertheless, the present model represents micro solvation involving a single explicit water molecule together with an implicit solvent description and does not fully account for cooperative interactions arising from multiple surrounding water molecules. Although the PCM model accounts for solvent polarization, the present study considers only a single water molecule interacting with scopoletin thus, the results should be interpreted as describing local water–scopoletin interactions rather than complete solvation.

To study the change distribution and electronic rearrangement accompanying the interaction of the water molecule with the scopoletin framework the Natural Population Analysis (NPA) of conformations (**C1** and **C2**) was investigated. In conformation **C1**, the water oxygen atom (O23) exhibits a significant negative charge of −1.02054 e, whereas the two hydrogen atoms (H24 and H25) show positive charges of +0.51240 e and +0.50104 e, respectively. These values deviate from those of an isolated water molecule, where oxygen generally carries around −0.997 e and hydrogen about +0.499 e, indicating pronounced polarization and strong hydrogen-bond involvement in the complex. The adjacent scopoletin oxygen atoms (O10–O13) possess moderately negative charges ranging from −0.525 to −0.690 e, consistent with their roles as potential hydrogen-bond acceptors, while nearby carbons such as C9 (+0.7576 e) and C14 (−0.3332 e) display substantial charge separation, typical of carbonyl or conjugated systems. The pronounced positive charge on the hydrogen atoms of the water molecule indicates that water primarily acts as a hydrogen-bond donor toward the oxygen-rich regions of scopoletin. At the same time, the negatively charged water oxygen can participate in weaker secondary electrostatic or lone-pair interactions with electrophilic carbon centers of the scopoletin framework. The very small contribution from Rydberg orbitals (approximately 0.29 %) further suggests that the interaction is dominated by electrostatic effects, with negligible charge-transfer or covalent character.[26]

In conformation **C2**, the carbon atoms exhibit moderate but systematic charge polarization. Ring carbons directly bonded to electronegative substituents carry positive natural charges, such as C2 (+0.356), C4 (+0.319), and C5 (+0.213), whereas carbons associated with π-electron density are correspondingly negative, with C1, C3, and C6–C8 ranging from –0.15 to –0.35. Among all carbon atoms, C9 shows the highest positive charge (+0.756), which is consistent with its location in a strongly electron-withdrawing environment. Oxygen atoms display substantial negative charges due to their high electronegativity and direct involvement in hydrogen bonding. The phenolic and lactone oxygen atoms possess charges in the range of –0.50 to –0.72, while the water oxygen (O23) carries the most negative charge (–1.019), reflecting significant localization of electron density on the interacting water molecule. Hydrogen atoms bonded to electronegative atoms show relatively large positive charges (0.50–0.54), supporting their role as effective

hydrogen-bond donors. The summed core and valence electron populations together account for more than 99 % of the total electron density, with only about 0.30 % arising from Rydberg contributions. This confirms a stable and physically meaningful electronic description without excessive diffuse character.[26] Overall, the NPA results clearly indicate charge redistribution upon complex formation, particularly in the vicinity of the interacting oxygen atoms, providing further evidence for stabilizing hydrogen-bonding interactions between water and scopoletin.

Natural Bond Orbital (NBO) analysis is an efficient approach for investigating intermolecular interactions by quantifying donor–acceptor charge transfer and the associated stabilization energies in molecular systems.[27] NBO analysis was performed for conformations **C1** and **C2** using their optimized geometries. The second-order perturbation (NBO) analysis for conformation **C1** (Table 2) reveals extensive intramolecular delocalization within the scopoletin scaffold together with a smaller but chemically significant set of intermolecular charge-transfer channels that stabilize the bound water molecule. Within the scopoletin unit, lone-pair → antibonding (LP → BD*) and bonding → antibonding (BD → BD*) delocalization are particularly large, for example LP(O11) → BD*(C9–O10) with delocalization energy of 39.15 kcal/mol and LP(O10) → BD*(C9–O11) with delocalization energy 35.61 kcal/mol. These delocalization's indicates strong resonance and electronic delocalization across the oxygenated/conjugated regions. Several delocalizations among the carbon framework are also sizable (e.g., BD (C3–C4) → BD* (C1–C2), with energy of 23.50 kcal/mol) and BD (C1–C2) → BD*(C5–C6) with energy of 19.18 kcal/mol), which together create a pre-polarized, resonance-stabilized binding pocket. Intermolecularly, the dominant donor–acceptor channel corresponds to lone-pair donation from a scopoletin oxygen (LP(O10)) into the antibonding O–H orbital of the water molecule i.e. BD*(O23–H24) with delocalization energy of 3.63 kcal/mol. Reciprocal charge transfer from the water into scopoletin is present but smaller in magnitude for example BD(O23–H24) → RY*(O10) with energy 0.63 kcal/mol and BD(O23–H25) → RY*(O10) with energy 0.21 kcal/mol, consistent with a primarily unidirectional LP → BD* stabilization that reinforces the H-bond without inducing covalent reorganization. A weak intermolecular interaction involving water oxygen LP(O23) → BD*(C3–H15) is also observed with energy of 1.27 kcal/mol, reflecting a small back-donation path to the scaffold. Overall, the NBO results quantitatively support an interaction dominated by hydrogen bonding and electrostatic polarization, reinforced by the intrinsic delocalization of the scopoletin electronic structure in conformation **C1**. Major donor acceptor interactions along with energy are shown in Table 2.

Second-order NBO analysis for conformation **C2** (Table 3) reveals a dominant intermolecular hydrogen bonding motif between scopoletin and water. The largest intermolecular stabilization is LP (O23) → BD*(O12–H19) with energy of 21.04 kcal/mol, this interaction corresponds to electron donation from the water oxygen lone pair into the antibonding orbital of the O12–H19 bond of scopoletin. This intermolecular interaction in **C2** is much larger as compared to confirmation **C1** (3.63 kcal/mol) indicating a stronger donor–acceptor interaction in **C2** and providing electronic-structure evidence for the stronger intermolecular interaction observed for C2. A secondary but notable interaction is LP(O13) → BD*(O23–H24) with energy of 5.91 kcal/mol, indicating additional donor–

Table 2. Second order perturbation theory analysis of Fock matrix in NBO basis for conformation **C1**.

No.	Donor	Acceptor	*E*(2) (kcal/mol)
1	LP(O11)	BD*(C9–O10)	39.15
2	LP(O10)	BD*(C9–O11)	35.61
3	BD (C3–C4)	BD* (C1–C2)	23.50
4	BD (C1–C2)	BD* (C5–C6)	19.18
5	BD (C1–C2)	BD* (C7–C8)	17.31
6	BD (C5–O13)	BD*(C5–C6)	7.5
7	LP(O10) (scopoletin)	BD*(O23–H24) (water)	3.63
8	BD(O23–H24) (water)	RY*(O10) (scopoletin)	0.63
9	BD(O23–H25) (water)	RY*(O10) (scopoletin)	0.21
10	BD(C3–H15) (scopoletin)	BD*(O23–H25) (water)	0.13
11	LP(O10) (scopoletin)	RY*(O23) (water)	0.06
12	LP (O23) (water)	BD*(C3–H15) (scopoletin)	1.27

acceptor charge transfer involving the water O–H bond. The intramolecular NBO analysis for **C2** shows many interactions with high stabilization energy reflecting strong electron delocalization in scopoletin and explain why charge redistribution on oxygens is readily accommodated upon complexation (Table 3). In conformation **C2** the LP (C1) donor orbital corresponds to a π-type p_z electron pair localized on the bridgehead C1 atom within the single-reference Lewis structure generated by the default NBO algorithm. The exceptionally high second-order perturbation stabilization energies $E(2)$ = 51.2 – 77.5 kcal/mol into the adjacent BD*(2)C2–C3, BD*(2)C5–C6, and BD*(2)C7–C8 orbitals reflect strong resonance delocalization, recovering the delocalized aromatic character of the bicyclic coumarin core (Table 3).

Overall, the NBO results indicate that the interaction between scopoletin and water is predominantly governed by electrostatic hydrogen bonding with measurable lone-pair → antibonding (LP→BD*) charge transfer. The stronger LP (O23) (water) → BD*(O12–H19) interaction in conformation **C2** (21.04 kcal/mol), compared with the LP(O10) → BD*(O23–H24) interaction in **C1** (3.63 kcal/mol), demonstrates that the conformational arrangement strongly influences hydrogen-bond strength and is consistent with the more negative interaction energy obtained for **C2**. Similar donor–acceptor interactions have been reported for apigenin–water complexes, where hydroxyl groups act as the preferred hydrogen-bond donor sites and exhibit stabilization energies in the range of 15–30 kcal/mol, consistent with the present results.[28] Likewise, DFT investigations of hydroxycoumarin–water complexes have shown that hydroxyl donor interactions are energetically more favorable than carbonyl or ether oxygen acceptor interactions, supporting the stronger interaction observed for **C2**.[28] Furthermore, the large intramolecular delocalization energies (30–77 kcal/mol) are comparable to those reported for other coumarin derivatives, confirming that extensive electron delocalization is an intrinsic feature of the coumarin framework and facilitates hydrogen-bond formation with water.[29–30]

To obtain a comprehensive description of noncovalent interactions in conformation **C1** and **C2** of the scopoletin–water complex, the reduced density gradient (RDG) scatter plot was analyzed together with the corresponding noncovalent interaction (NCI) isosurface visualization. While the RDG scatter plot provides a quantitative classification of interactions based on the sign(λ_2)ρ descriptor, the NCI isosurface plot offers real-space localization of these interactions between specific atoms. The colored scattered plot between reduced density gradient (RDG) and sign(λ_2)ρ along with RDG isosurface of conformation **C1** is shown in Figure 4. In the RDG scatter plot, regions with low RDG values and negative sign(λ_2)ρ (blue to green color range) indicate attractive interactions. These features correspond directly to the blue–green NCI isosurfaces observed between the water hydrogen (H24) and the scopoletin oxygen atom (O10). This spatial overlap confirms the presence of an O–H···O hydrogen bond, in which scopoletin acts as the hydrogen-bond acceptor and water as the donor. The moderate intensity and limited spatial extent of the blue region suggest a weak to moderate hydrogen bond, consistent with the NBO-derived LP(O10) → BD*(O23–H24) interaction and moderate charge transfer. The green region cantered near sign(λ_2)ρ ≈ 0 in the scatter plot corresponds to weak van der Waals interactions. In the NCI isosurface representation, these interactions appear as diffuse green surfaces surrounding the water molecule and the aromatic π-system of scopoletin. Such surfaces indicate dispersive contacts between the water oxygen (O23), water hydrogens, and the π-electron cloud of the benzene ring. These interactions are non-directional and contribute to stabilization through weak dispersion rather than

Table 3. Second order perturbation theory analysis of Fock matrix in NBO basis for conformation **C2**.

No.	Donor NBO (unit)	Acceptor NBO (unit)	$E(2)$ (kcal/mol)
1	LP (O23) (water)	BD*(O12–H19) (scopoletin)	21.04
2	LP (O13) (scopoletin)	BD*(O23–H24) (water)	5.91
3	BD(O12–H19) (scopoletin)	BD*(O23–H25) (water)	0.22
4	BD(O23–H24) (water)	BD*(O12–H19) (scopoletin)	0.76
5	LP (C1)	BD*(C5–C6)	74.3
6	LP (C1)	BD*(C7–C8)	51.2
7	LP (C1)	BD*(C2–C3)	77.5
8	LP (O12)	BD*(C4–C5)	53.95
9	LP (O11)	BD*(C8–C9)	16.4
10	LP (O11)	BD*(C9–O10)	39.8

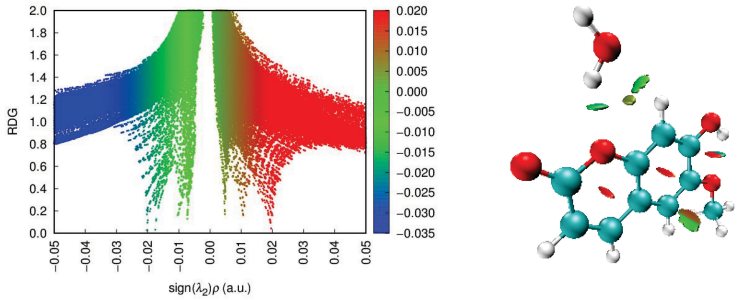


Figure 4. The coloured scattered plot between reduced density gradient (RDG) and sign(λ_2)ρ and RDG isosurface of conformation **C1**

electrostatics or charge transfer. Conversely, the red regions at positive sign(λ_2)ρ values in the RDG scatter plot signify steric repulsion. These features correlate with red NCI isosurfaces localized within the scopoletin framework, particularly around closely packed ring carbons and substituent groups. These repulsive interactions arise from Pauli exclusion due to electron density overlap and reflect intrinsic intramolecular strain rather than intermolecular effects. Importantly, neither the scatter plot nor the isosurface visualization shows sharp features at strongly negative sign(λ_2)ρ values or intense deep-blue isosurfaces. This confirms the absence of strong covalent or highly directional interactions in conformation **C1**. Instead, the stabilization of the complex is governed by a combination of weak hydrogen bonding, van der Waals interactions, and steric effects, characteristic of noncovalently bound molecular assemblies.

The reduced density gradient (RDG) scatter plot and corresponding noncovalent interaction (NCI) isosurface in conformation **C2** of the scopoletin–water complex is shown in Figure 5. In the RDG scatter plot for conformation **C2**, a prominent accumulation of points at low RDG values (RDG < 0.4) and significantly negative sign(λ_2)ρ is observed. This feature indicates the presence of stronger attractive interactions as compared to **C1**. These negative sign(λ_2)ρ regions correspond directly to intense blue NCI isosurfaces localized between the scopoletin hydroxyl group (O12–H19) and the water oxygen atom (O23). This clearly identifies a strong O–H···O hydrogen bond, in which scopoletin acts as the hydrogen-bond donor and water functions as the hydrogen-bond acceptor. The increased intensity and spatial continuity of the blue isosurface confirm a stronger and more directional hydrogen bond in conformation **C2**. In addition to this primary interaction, the RDG scatter plot displays secondary features near slightly negative to near-zero sign(λ_2)ρ values, corresponding to green NCI isosurfaces (Figure 5). These are distributed between the water molecule and nearby scopoletin oxygen atoms as well as over the aromatic π-system. These features indicate auxiliary hydrogen-bonding and van der Waals interactions, suggesting a cooperative or bifurcated hydrogen-bond network in which water simultaneously interacts with multiple electro-negative sites of scopoletin. Such cooperativity is consistent with the NBO results for **C2**, which show multiple donor–acceptor channels with appreciable stabilization energies. The red regions at positive sign(λ_2)ρ values in the RDG scatter plot correspond to steric repulsion, and their associated red NCI isosurfaces are primarily confined within the scopoletin molecular framework. These repulsive interactions arise from close intramolecular contacts among ring atoms and substituents and do not directly

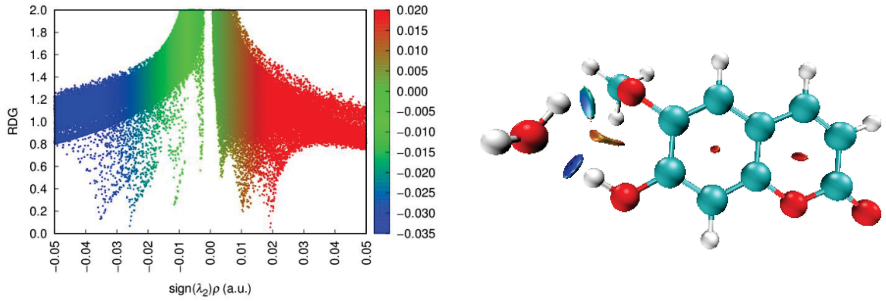


Figure 5. The coloured scattered plot between reduced density gradient (RDG) and sign(λ_2)ρ and RDG isosurface of conformation **C2.**

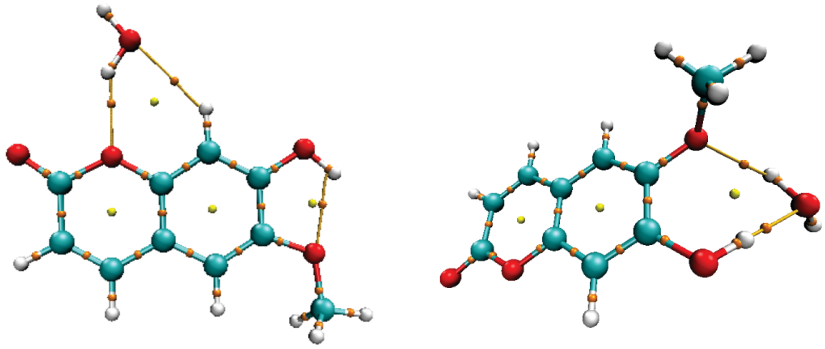


Figure 6. AIM analysis of conformations **C1** and **C2** showing attractors and various critical points (color scheme: attractors-purple, BCP– magenta, RCP– yellow and CCP– green).

contribute to intermolecular binding. Notably, the RDG plot for **C2** exhibits stronger and more clearly defined negative sign(λ_2)ρ features than **C1**, and the NCI isosurface shows larger and more intense blue regions. This demonstrates that conformation **C2** is stabilized by stronger hydrogen bonding and enhanced electrostatic attraction, whereas dispersion and steric interactions play supporting roles. The absence of extremely sharp spikes at very negative sign(λ_2)ρ values indicates that the interaction remains noncovalent in nature, without significant covalent bond formation.

The nature and strength of the interactions between water and scopoletin in conformations **C1** and **C2** were further characterized using the Quantum Theory of Atoms in Molecules (QTAIM). The analysis was performed at the bond critical points (BCPs) associated with intermolecular contacts, and key topological descriptors including the electron density (ρ_{BCP}), Laplacian of electron density ($\nabla^2\rho_{BCP}$), total energy density (H_{BCP}), ellipticity (ε), and hydrogen-bond energy (E_{HB}) were evaluated. The bond energy of hydrogen bond was estimated by using empirical correlation $-223.08 \times \rho_{BCP}$/a. u. + 0.7423 kcal/mol which relates the hydrogen-bond energy to the electron density at the bond critical point.[31] The AIM analysis of conformation **C1** and **C2** is shown in Figure 6. The values of topological parameters i.e. electron density (ρ), its Laplacian $\nabla^2\rho$, local electronic energy density (H_{BCP}), and ellipticity (ε) for some important bond interactions are shown in Table 4.

In conformation **C1**, two intermolecular bond paths are identified for water-scopoletin complex between hydrogen atom of aromatic ring (H15) and oxygen atom of water (O23) i.e. H15···O23 and between hydrogen atom of water (H24) and oxygen atom of scopoletin (O10) i.e. H24···O10. The corresponding H···O bond lengths are 2.517 Å and 2.101 Å, with bond angles of 172.43° and 143.23°, respectively. The shorter H24···O10 bond distance indicates a relatively stronger hydrogen-bonding interaction than H15···O23. The electron density values at the corresponding to interaction between H15···O23 is 0.007367 with Laplacian of electron density of 0.027923, which is characteristic of weak hydrogen bonding. The positive values of the $\nabla^2\rho_{BCP}$ indicate closed-shell interactions dominated by electrostatic forces, consistent with conventional hydrogen bonding. The hydrogen bond energy of this interaction was estimated to be −0.90 kcal/mol. For interaction between H24···O10 the value of electron density and its Laplacian was found to be 0.017547 and 0.054744 respectively. These values suggest moderate to strong hydrogen bond interaction which stabilize conformation **C1**. The hydrogen bond energy for this interaction was estimated to be −3.17 kcal/mol. The ellipticity values (ε) provide additional information on the anisotropy of the electron density at the corresponding BCPs. Conformation **C2** also exhibits two intermolecular hydrogen bonds between the scopoletin and water molecules. The first interaction involves the hydroxyl

Table 4. Topological and geometrical parameters of interaction between water and scopoletin.

Conformation	Interaction	Bond length (Å)	Bond angle (°)	ρ_{BCP}	$\nabla^2\rho_{BCP}$	H_{BCP}	ε	E_{HB} (kcal/mol)
C1	H15-O23	2.517	172.43 (H15···O23–H25)	0.007367	0.027923	0.0009677	0.035905	–0.90
	H24-O10	2.101	143.23 (O23–H24···O10)	0.017547	0.054744	–0.001493	0.056412	–3.17
C2	H19-O23	1.787	179.15 (O12–H19···O23)	0.035681	0.103401	0.000008	0.036435	–7.22
	H24-O13	1.910	140.23 (O23–H24···O13)	0.025951	0.079328	–0.000775	0.148886	–5.05

hydrogen of scopoletin (H19) forming a hydrogen bond with the oxygen atom of water (O23) i.e. H19···O23, while the second interaction arises between a hydrogen atom of water (H24) and the oxygen atom of scopoletin (O13) i.e. H24···O13. The H19···O23 interaction possesses the shortest H···O bond distance (1.787 Å) and an almost linear O12–H19···O23 bond angle (179.15°), indicating a strong and highly directional hydrogen bond. In contrast, the H24···O13 interaction has a bond length of 1.910 Å and a bond angle of 140.23°, corresponding to a moderately strong hydrogen bond. For the H19···O23 interaction, the electron density at the bond critical point (BCP) is 0.035681 a.u., accompanied by a Laplacian of electron density of 0.103401 a.u. These comparatively high values are indicative of a strong hydrogen bond, while the positive Laplacian confirms that the interaction belongs to the closed-shell category and is primarily electrostatic in nature. The corresponding hydrogen-bond energy was estimated to be −7.22 kcal/mol, identifying this interaction as the dominant stabilizing contribution in conformation **C2**. The second interaction, H24···O13, exhibits an electron density of 0.025951 a.u. and a Laplacian value of 0.079328 a.u. at the BCP, which are characteristic of a moderate-to-strong hydrogen bond. The hydrogen-bond energy estimated for this interaction is −5.05 kcal/mol, demonstrating that it also contributes significantly to the stabilization of the complex. The relatively low ellipticity (ε) values for both bond paths suggest that the electron density is well localized along the interaction lines, reflecting the directional and structurally well-defined nature of these hydrogen bonds. Collectively, these results show that conformation **C2** exhibits fewer but substantially stronger hydrogen-bonding interactions than **C1**, consistent with its more negative interaction energy.

The QTAIM results obtained in the present study are consistent with previous investigations of structurally related flavonoid– and coumarin–water complexes. Zheng et al.[32] reported that in luteolin and water complexes, stronger O–H···O hydrogen bonds exhibit higher electron density at the bond critical point together with larger NBO stabilization energies than C–H···O interactions, a trend that agrees well with the present results, where the O–H···O interaction in C2 (H19···O23, E_{HB} = −7.22 kcal/mol) is considerably stronger than the C–H···O interaction in C1 (H15···O23, E_{HB} = −0.90 kcal/mol). Similarly, DFT/QTAIM studies have reported O–H···O hydrogen-bond distances and interaction energies of comparable magnitude for example, an O–H···O=C intramolecular hydrogen bond distance of 1.739 Å with an associated binding energy of −14.00 kcal/mol has been reported for a luteolin–water complex supporting the reliability of the present calculations, with the somewhat smaller magnitude of the intermolecular H19···O23 interaction found here (1.787 Å, −7.22 kcal/mol) being consistent with the expected distinction between resonance-assisted intramolecular and simple intermolecular O–H···O hydrogen bonds.[32] According to the commonly accepted classification of hydrogen-bond strengths based on QTAIM and spectroscopic studies,[33] the H15···O23 interaction corresponds to a very weak hydrogen bond, whereas the H24···O10, H24···O13, and H19···O23 interactions fall within the weak-to-moderate hydrogen-bond regime. These observations are in good agreement with the calculated QTAIM descriptors and estimated hydrogen-bond energies, supporting the presence of stronger hydrogen-bonding interactions in **C2** compared with the other investigated conformers.

CONCLUSIONS

A comprehensive DFT investigation of the scopoletin–water complex was carried out at the B3LYP-D3(BJ)/6-311++G(d,p) level of theory. A systematic conformational search identified five stable binding motifs (**C1–C5**), with conformation **C2** exhibiting the most negative interaction energy in both the gas phase and the PCM aqueous environment considered for **C1** and **C2**. The calculated interaction energies, including BSSE and ZPE corrections, indicate that **C2** possesses the strongest intermolecular interaction among the investigated conformers. NPA, NBO, RDG, and QTAIM analyses consistently demonstrated that the intermolecular interactions are governed predominantly by electrostatic O–H···O hydrogen bonding accompanied by moderate LP→BD* charge transfer. The stronger and more directional hydrogen-bonding interactions in C2 are consistent with its more negative interaction energy relative to the other conformers. Overall, the present study provides detailed molecular-level insight into the microsolvation of scopoletin and establishes a reliable theoretical framework for understanding hydrogen-bonding interactions in coumarin-based systems. These findings may serve as a useful basis for future investigations involving explicit solvent models and biologically relevant environments for investigating hydrogen-bonding interactions in coumarin-based systems.

REFERENCES

[1] H. Guo, M. Li, M.-H. Li, J. Cui, L. Wang, J. Yang, Z. Ma, Z. Wang, J. Li, W. Huan, *Microchem. J.* **2026**, *225*, 118162. https://doi.org/10.1016/j.microc.2026.118162.

[2] X.-Y. Gao, X.-Y. Li, C.-Y. Zhang, C.-Y. Bai, *Front. Pharmacol.* **2024**, *15*, 1268464. https://doi.org/10.3389/fphar.2024.1268464.

[3] F. C. Torres, N. Brucker, S. Fernandes Andrade, D. Fabio Kawano, S. Cristina Garcia, G. Lino von Poser, V. Lucia Eifler-Lima, *Curr. Top. Med. Chem.* **2014**, *14*, 2600–2623.
[4] P. Ball, *Chem. Rev.* **2008**, *108*, 74–108. https://doi.org/10.1021/cr068037a.
[5] a) S. Ganai, P. Mukherjee, K. Mahali, A. Saha, A. Hossain, A. V. Soldatov, A. M. A. Henaish, J. Ahmed, S. Roy, *New J. Chem.* **2023**, *47*, 13547–13557. https://doi.org/10.1039/d3nj02412a.
b) A. Adhikari, W.-W. Park, O.-H. Kwon, *ChemPlusChem*, **2020**, *85*, 2657–2665. https://doi.org/10.1002/cplu.202000744.
[6] S. M. Cybulski, C. E. Seversen, *J. Chem. Phys.* **2005**, *122*, 014117. https://doi.org/10.1063/1.1829044.
[7] Y. Cho, W. J. Cho, I. S. Youn, G. Lee, N. J. Singh, K. S. Kim, *Acc. Chem. Res.* **2014**, *47*, 3321–3330. https://doi.org/10.1021/ar400326q.
[8] A. E. Reed, R. B. Weinstock, F. Weinhold, *J. Chem. Phys.* **1985**, *83*, 735–746. https://doi.org/10.1063/1.449486.
[9] A. E. Reed, L. A. Curtiss, F. Weinhold, *Chem. Rev.* **1988**, *88*, 899–926. https://doi.org/10.1021/cr00088a005.
[10] E. R. Johnson, S. Keinan, P. Mori-Sánchez, J. Contreras-García, A. J. Cohen, W. Yang, *J. Am. Chem. Soc.* **2010**, *132*, 6498–6506. https://doi.org/10.1021/ja100936w.
[11] J. Contreras-García, E. R. Johnson, S. Keinan, R. Chaudret, J. P. Piquemal, D. N. Beratan, W. Yang, *J. Chem. Theory Comput.* **2011**, *7*, 625–632. https://doi.org/10.1021/ct100641a.
[12] R. F. W. Bader, Atoms in Molecules: A Quantum Theory, Oxford Univ. Press, **1990**.
[13] U. Koch, P. L. A. Popelier, *J. Phys. Chem.* **1995**, *99*, 9747–9754. https://doi.org/10.1021/j100024a016.
[14] C. D. Zeinalipour-Yazdi, *J. Mol. Model.* **2022**, *28*, 285. https://doi.org/10.1007/s00894-022-05258-w.
[15] N. Elangovan, N. Arumugam, M. Thirumavalavan, S. Q. Sabarimuthu, R. Padmanaban, J. Bhagavathsingh, S. Mathew, *J. Mol. Liq.* **2024**, *406*, 125150. https://doi.org/10.1016/j.molliq.2024.125150.
[16] H. Wang, Z. Huang, T. Shen, L. Guo, *J. Mol. Model.* **2012**, *18*, 3113–3123. https://doi.org/10.1007/s00894-011-1325-8.
[17] M. J. Frisch et al., Gaussian 09, Revision A.02, Gaussian Inc., Wallingford CT, **2016**.
[18] R. Dennington, T. A. Keith, J. M. Millam, GaussView, Version 6, **2016**.
[19] T. Lu, F. Chen, *J. Comput. Chem.* **2012**, *33*, 580–592. https://doi.org/10.1002/jcc.22885.
[20] W. Humphrey, A. Dalke, K. Schulten, *J. Mol. Graph.* **1996**, *14*, 33–38. https://doi.org/10.1016/0263-7855(96)00018-5.
[21] R. A. Boto, J. P. Piquemal, J. Contreras-García, *Theor. Chem. Acc.* **2017**, *136*, 1. https://doi.org/10.1007/s00214-017-2169-9.
[22] R. F. W. Bader, H. H. Essén, *J. Chem. Phys.* **1984**, *80*, 1943–1960. https://doi.org/10.1063/1.446956.
[23] K. B. Wiberg, P. R. Rablen, *J. Comput. Chem.* **1993**, *14*, 1504–1518. https://doi.org/10.1002/jcc.540141213.
[24] A. Joseph, V. I. Thomas, G. Żyła, A. S. Padmanabhan, S. Mathew, *J. Phys. Chem. A* **2018**, *122*, 328–340. https://doi.org/10.1021/acs.jpca.7b09189.
[25] J. Tomasi, M. Persico, *Chem. Rev.* **1994**, *94*, 2027–2094. https://doi.org/10.1021/cr00031a013.
[26] J. Simons, *J. Chem. Phys.* **2022**, *156*, 100901. https://doi.org/10.1063/5.0084574.
[27] F. Weinhold, *J. Comput. Chem.* **2012**, *33*, 2363–2379. https://doi.org/10.1002/jcc.23060.
[28] Y.-Z. Zheng, Y. Zhou, Q. Liang, D.-F. Chen, R. Guo, R.-C. Lai, *Sci. Rep.* **2016**, *6*, 34647. https://doi.org/10.1038/srep34647.
[29] J. Li, Z. Zhang, H. Sun, Y. Wang, X. Kahaer, D. Aizezi, M. Xiang, B. Abulimiti, *J. Mol. Model.* **2026**, *32*, 38. https://doi.org/10.1007/s00894-025-06615-1.
[30] C. Ait-Ramdane-Terbouche, H. Abdeldjebar, A. Terbouche, H. Lakhdari, K. Bachari, T. Roisnel, D. Hauchard, *J. Mol. Struct.* **2020**, *1222*, 128918. https://doi.org/10.1016/j.molstruc.2020.128918.
[31] S. Emamian, T. Lu, H. Kruse, H. Emamian, *J. Comput. Chem.* **2019**, *40*, 2868–2881. https://doi.org/10.1002/jcc.26068.
[32] Y.-Z. Zheng, Y. Zhou, Q. Liang, D.-F. Chen, R. Guo, *J. Mol. Model.* **2016**, *22*, 257. https://doi.org/10.1007/s00894-016-3128-4.
[33] A. V. Afonin, D. Rusinska-Roszak, *J. Mol. Model.* **2024**, *30*, 18. https://doi.org/10.1007/s00894-023-05811-1.